*Physicochem. Probl. Miner. Process., 62(4), 2026, 226052*

http://www.journalssystem.com/ppmp

Physicochemical Problems of Mineral Processing

ISSN 1643-1049


# Performance assessment of a flaxseed-derived bioflocculant for solid-liquid separation in mineral processing: optimization of extraction conditions and mechanistic insights with application to the phosphate industry

**Mohamed Sakkali [1,2], Mohamed EL Khouakhi [2], Rachid Bagoun [1,2], Khamis El Kandoussi [2], Abdelmoughit Abidi [2,3], Mohammed El Asri [1,2], Ahmed Boulahna [1]**

[1] Laboratory of Applied Organic Chemistry, Faculty of Science and Techniques, University of Sidi Mohamed Ben Adbellah, Morocco

[2] Technology Development Cell (TechCell), Mohammed VI Polytechnic University (UM6P), Benguerir, Morocco

[3] Applied Chemistry and Biomass Team, Cadi Ayyad University, Morocco

Corresponding author: mohamed.sakkali@usmba.ac.ma (Mohamed Sakkali)

**Abstract:** This study evaluates the performance of a flaxseed-derived bioflocculant for solid–liquid separation in mineral processing, focusing on phosphate concentrate and phosphate sludge. A Design of Experiments (DoE) approach was employed to optimize a simple and scalable aqueous extraction process by assessing the effects of key parameters, including extraction temperature, seed loading, agitation speed, residence time, NaCl concentration, and dilution injection mode. The results demonstrate that a single optimized extraction condition yields an effective bioflocculant suitable for both phosphate matrices. Among the studied factors, seed loading, extraction temperature, agitation speed, residence time, and dilution injection mode were identified as the most influential variables affecting extraction yield and flocculation efficiency. The predictive models exhibited excellent accuracy ($R^2$ > 99%), confirming the robustness of the optimization strategy. Sedimentation tests showed a marked improvement in settling kinetics in both matrices, with performance comparable to conventional polyacrylamide-based flocculants. Optimal dosages were approximately 400 g/t for phosphate concentrate and 205 g/t for phosphate sludge. An injection concentration of 0.5 g/L was found to provide an optimal balance between flocculation efficiency and water usage. Chemical characterization revealed a complex composition of organic acids, phenolic compounds, flavonoids, and lignans. Zeta potential measurements indicated that both particles and bioflocculant remained negatively charged, suggesting that flocculation is governed primarily by a polymer bridging mechanism, supported by hydrogen bonding interactions. Overall, flaxseed-derived bioflocculants represent a sustainable and efficient alternative for mineral processing and water recovery applications.

***Keywords:*** mineral processing, phosphate dewatering, bioflocculant, flaxseed, design of experiment, screening design

## 1. Introduction

Sustainable water management represents a critical challenge in the mining industry, particularly in arid and semi-arid regions where water scarcity necessitates improved recycling strategies and reduced freshwater consumption (Arenas-Collao et al., 2024; De Lima et al., 2025). Phosphate beneficiation is predominantly based on wet process routes, which are inherently water-intensive, thereby requiring efficient water recovery systems, such as thickeners, to mitigate environmental impacts and ensure process sustainability (Bergani, Taha, et al., 2025).

Flocculation and sedimentation play a central role in these systems by promoting particle aggregation and accelerating settling rates, directly influencing water clarification and recycling (Bergani, Ait-Khouia, et al., 2025; Bergani, Taha, et al., 2025). Synthetic flocculants, particularly

DOI: 10.37190/ppmp/226052

polyacrylamide-based polymers, are widely used due to their high performance. However, their limited biodegradability and potential environmental risks have raised increasing concerns, driving the search for more sustainable and eco-compatible alternatives (Bergani, Taha, et al., 2025; Elrasoul & Yong, 2025; Orchard et al., 2024).

In this regard, bioflocculants derived from natural sources have garnered heightened interest as environmentally friendly alternatives, delivering similar efficacy while enhancing ecological compatibility. Their application in mineral processing has expanded recently, especially in tailings management and water recovery operations (Bergani, Ait-Khouia, et al., 2025b; Bergani, Taha, et al., 2025).

Among these, flaxseed (Linum usitatissimum) has emerged as a promising bioflocculant precursor due to its high content of hydrophilic polysaccharides, notably mucilage, which exhibits strong flocculating properties and a high affinity for fine particles. Flaxseed-derived extracts have been extensively investigated in wastewater treatment, where they have demonstrated significant effectiveness in turbidity reduction and water clarification (Venegas-García & Wilson, 2022).

A previous study has demonstrated the potential of flaxseed-based bioflocculants for the settling phosphate slurries from the Youssoufia washing plant in Morocco (Ettoumi et al., 2025). In that study, mucilage was extracted through a multistep process involving sieving, washing, and thermal extraction (70 °C, 60 min, S/L = 1:10) using distilled water, followed by centrifugation. Two products were obtained: a crude bioflocculant (F1), initially produced after freezing at −20 °C for 3 days, which required relatively high dosages (800–900 g/t). Extending the freeze-drying time to 5 days significantly reduced the required dosage to approximately 200 g/t. A second product (F2) was obtained through ethanol (95%) precipitation (1 h, S/L = 1:3), followed by freeze-drying for 3 days and subsequent grinding.

In contrast, the present study investigates a flaxseed-derived bioflocculant for application to two distinct phosphate matrices: phosphate sludge and phosphate concentrate. The primary objective is to optimize the extraction process using a simplified and cost-effective approach based solely on thermal extraction and filtration, without recourse to centrifugation, solvent precipitation, or freeze-drying. This strategy aims to reduce process complexity, processing time, and operational cost while identifying the most suitable extract for each matrix. In addition, flocculant injection parameters, including dosage and concentration, are optimized to improve sedimentation performance while minimizing bioflocculant consumption.

## 2. Materials and methods

### 2.1. Industrial context and sample collection

#### 2.2.1. Description of the phosphate beneficiation process

The present study was carried out based on the industrial flowsheet of a phosphate washing plant located in the Khouribga basin (Morocco). The beneficiation process follows a wet route including screening, hydraulic classification, grinding, flotation, and thickening operations with internal water recycling (Fig. 1).

Following slurry preparation, the ore is first screened at 2.5 mm. The coarse fraction is rejected as waste, whereas the undersize fraction undergoes size classification, starting with a cut size of 400 µm. The 400 µm–2.5 mm fraction, corresponding to the coarse concentrate, is subjected to grinding to achieve the particle size required for pipeline transport.

The fraction finer than 400 µm is subsequently processed by hydrocycloning with a secondary cut at 160 µm. The 160–400 µm fraction is further ground prior to flotation, while the 40–160 µm fraction is directly fed to the flotation circuit. A third classification stage at 40 µm, performed using a hydrocyclone, enables the removal of ultrafine particles before flotation.

The ultrafine fraction (< 40 µm), originating from both desliming and hydrocycloning stages, is directed to the sludge thickening circuit. Flotation is conducted through an indirect method to produce a purified phosphate concentrate (PC). The resulting concentrate is subsequently blended with the previously ground coarse fraction (400 µm–2.5 mm) and transferred to the concentrate thickener. In parallel, non-floated particles from the flotation stage are conveyed to the sludge thickener.

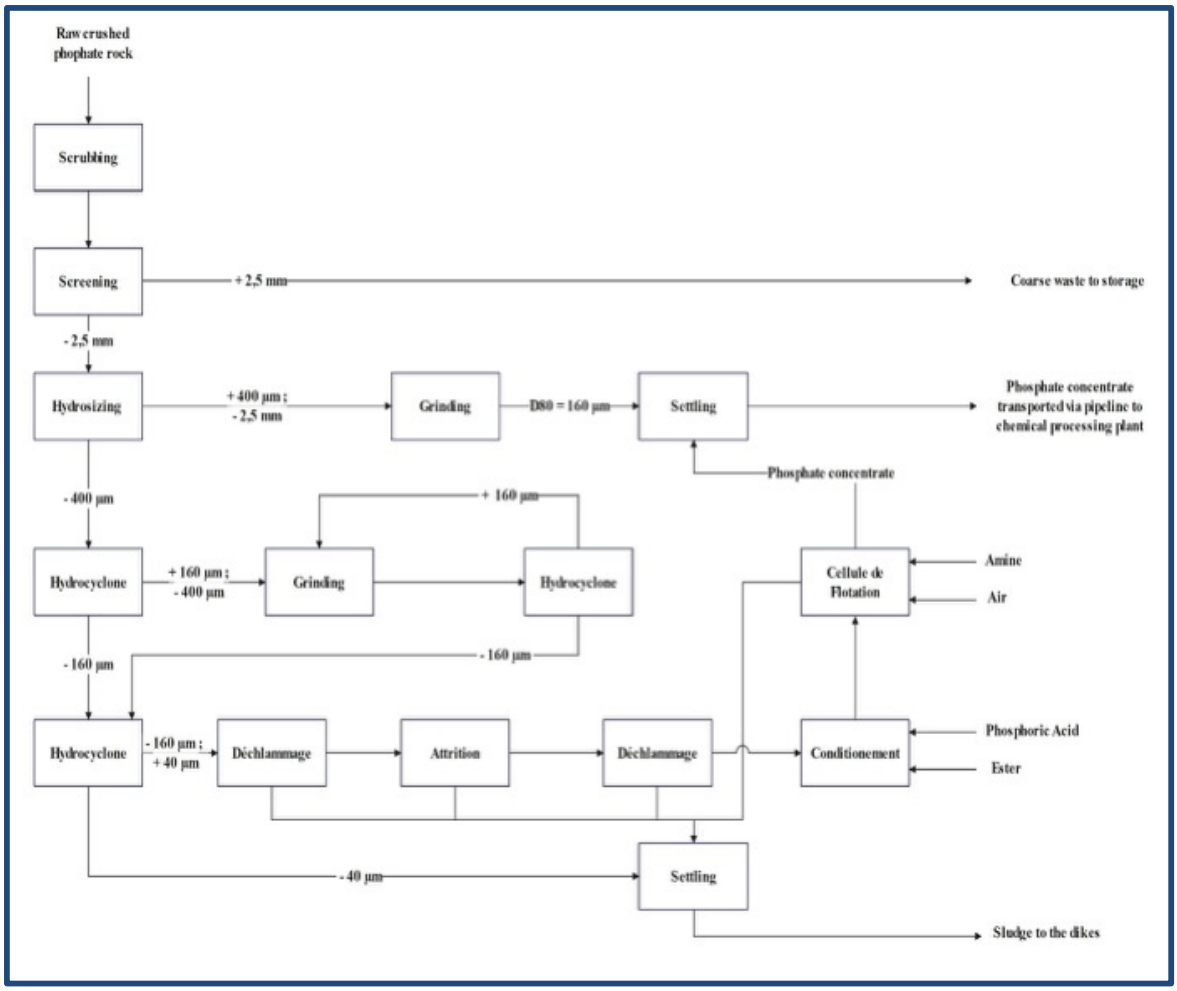


Fig. 1. Flowsheet of the Merah phosphate beneficiation plant

Phosphate sludge (PS) is treated with a synthetic flocculant for concentrate (SFC) to improve settling and attain the necessary solids concentration for subsequent transport. Similarly, fine sludge undergoes treatment with a synthetic flocculant for sludge (SFS) to enhance sedimentation before disposal. These thickening processes facilitate effective water recovery, allowing the clarified water to be reused within the processing facility, thus diminishing freshwater usage.

### 2.1.2. Sampling strategy and industrial slurry collection

Two types of slurries were collected from the industrial site:

- A concentrate slurry originating from the phosphate beneficiation circuit, characterized by a particle size distribution with D80 of approximately 160 µm.
- A refined tailings slurry representative of the residual stream produced from desliming, non-floating fractions, and fine particulates, predominantly composed of particles smaller than 40 µm.

Sampling was performed at the inlet of each thickener, upstream of the flocculant injection point, in order to ensure the absence of added polymer and accurately reflect the native physicochemical state of the industrial suspensions.

### 2.1.3. Laboratory reconstitution and solid concentration adjustment

In laboratory experiments, the solid concentration of the suspensions was adjusted to values lower than those encountered under industrial conditions in order to mitigate sampling constraints, reduce material consumption, and ensure experimental reproducibility.

To this end, a reconstitution protocol was implemented: the collected slurries were dried, then ground and sieved to get controlled and representative particle size distribution. Subsequently,

synthetic suspensions were prepared at reduced, yet representative, solid concentrations suitable for laboratory-scale investigations. This approach ensures that variations in flocculation behavior are predominantly governed by physicochemical interactions rather than differences in particle size distribution or solids content.

Importantly, this adjustment doesn't affect the validity of performance evaluation, as flocculant dosage is expressed per unit mass of solids (g/t of phosphate), thereby enabling consistent and meaningful comparisons across different experimental conditions.

### 2.2. Physicochemical characterization of phosphate materials

The chemical composition of the raw materials was determined by X-ray fluorescence spectroscopy (XRF, Epsilon 4, Malvern Panalytical, UK). The particle size distribution of PC and PS was measured using a laser diffraction analyzer (Mastersizer 2000, Malvern Panalytical).

### 2.3. Flocculating agents

#### 2.3.2. Industrial synthetic flocculants

Laboratory experiments were carried out under conditions representative of industrial practice, including the type of polymer, preparation procedure, and flocculant dosages, in order to ensure the relevance and comparability of the results with plant operations.

Flocculant solutions were prepared using a standard scale-down protocol commonly employed in industry, involving the gradual addition of dry polymer to water under continuous agitation to promote homogeneous dispersion and complete hydration. The solution was mixed until uniform and subsequently used in sedimentation tests. The reference industrial dosages are summarized in Table 1.

Table 1. Industrial flocculant dosages used as reference conditions

| Flocculant | Type of phosphate particles | Specific consumption (g/t of solids) | Injection concentration (g/L) |
|---|---|---|---|
| SFS | PS | 11 | 0.02 |
| SFC | PC | 16 | 0.05 |

#### 2.3.3. Extraction and preparation of the flaxseed-based BF

The bioflocculant (BF) investigated in this study was extracted from flaxseed (Linum usitatissimum), selected for its high content of hydrophilic polysaccharides exhibiting strong flocculating properties. A hot aqueous extraction method was employed to solubilize these macromolecules through a simple, solvent-free process. Flaxseeds were introduced into preheated water at a controlled temperature, using a defined solid-to-liquid mass ratio. The suspension was maintained under continuous agitation for a specified duration to facilitate the diffusion of soluble compounds into the aqueous phase. Following extraction, the suspension was filtered to separate the solid residue from the liquid phase, the latter constituting the crude BF extract.

The extracted mass was determined by mass balance according to **Błąd! Nie można odnaleźć źródła odwołania.**:

$$m_{extracted} = m_{initial} - m_{residue\ dry} \quad (1)$$

The concentration of the BF in the filtrate was calculated based on the filtrate volume as expressed in **Błąd! Nie można odnaleźć źródła odwołania.**:

$$C_{BF} = \frac{m_{extracted}}{V_{filtrate}} \quad (2)$$

The required volume of the BF solution for the flocculation test was determined from the target specific consumption and the mass of the phosphate solids, according to **Błąd! Nie można odnaleźć źródła odwołania.**:

$$V_{BF} = \frac{CS * m_s}{C_{BF}} \quad (3)$$

where $V_{BF}$ is the volume of BF solution (L), $SC$ is the specific consumption of flocculant (g/t of phosphate solids), $m_s$ is the mass of phosphate solids used (t), and $C$ is the concentration of the BF solution (g/L).

### 2.4. Sedimentation experiments and determination of settling velocity

#### 2.4.2. Experimental procedure

Sedimentation tests were performed to assess the settling of phosphate suspensions with flocculants present. All experiments were conducted at ambient temperature utilizing a 1000 mL graduated cylinder, with ongoing observation and documentation of the settling process.

The experimental procedure included slurry preparation, flocculant solution formulation, and sedimentation assessments. Precisely, 80 g of the phosphate sample was dissolved in water and transferred to a cylinder to achieve a final volume of 1000 mL. The flocculant solution was prepared independently at the specified concentration and then added to the suspension following initial homogenization.

After gentle mixing, sedimentation kinetics were observed by measuring the height of the solid–liquid interface over time.

#### 2.4.3. Determination of settling velocity

The settling velocity ($\vartheta$) was selected as the primary response variable, as it provides a direct measure of flocculation efficiency and clarification performance (Jarvis et al., 2005). In contrast, turbidity measurements were considered less suitable under the present experimental conditions. The sedimentation behavior was interpreted based on Kynch's theory (Concha A., 2014).

Sedimentation was monitored by recording the evolution of the solid–liquid interface height as a function of time (Fig. 2). The resulting sedimentation curves displayed four distinct regions:

- **Domain 1 – Initial settling region**: The initially homogeneous suspension begins to destabilize, and the interface height decreases nonlinearly.
- **Domain 2 – Constant-rate settling region:** Floc formation reaches a stable state; the interface height decreases linearly with time, and the settling velocity remains constant.
- **Domain 3 – Hindered settling region**: Increased particle-particle interactions and flocculation lead to a progressive reduction in settling velocity.
- **Domain 4 – Compression region**: The accumulated solids undergo compression under their own weight, forming a denser, semi-rigid network.

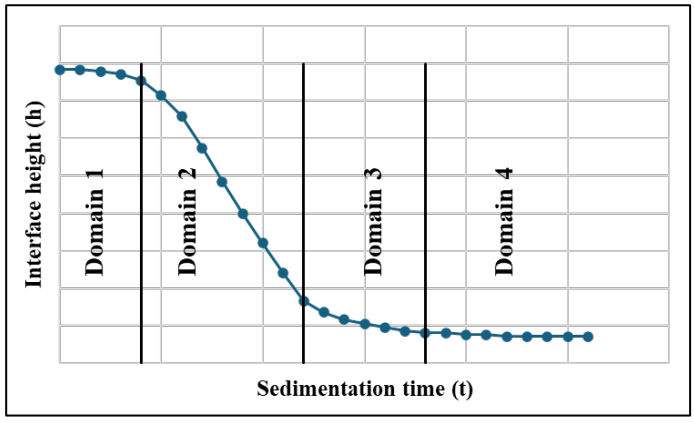


Fig. 2. General shape of the sedimentation curve

The settling velocity ($\vartheta$) was determined from the slope of the linear portion (Domain 2) of the height–time curve, according to **Błąd! Nie można odnaleźć źródła odwołania.**:

$$\vartheta = -\frac{\mathrm{dH}}{\mathrm{dt}} \tag{4}$$

where $H$ is the height of the solid-liquid interface and $t$ is time.

### 2.5. Flocculant contribution

To evaluate the performance of the BF in PC and PS, the relative contribution of the flocculant to the overall sedimentation velocity was quantified. This parameter enables isolation of the specific effect of flocculation on settling behavior.

The flocculant contribution was calculated according to Eq. (5):

$$\text{Flocculant Contribution (\%)} = \frac{V_{with} - V_{without}}{V_{with}} \times 100 \quad (5)$$

where $V_{with}$ and $V_{without}$ represent sedimentation velocities measured in the presence and absence of flocculant, respectively.

### 2.6. Experimental design and optimization strategy

#### 2.6.2. Screening design for BF extraction optimization

A design of experiments (DoE) approach was implemented to optimize the aqueous extraction conditions of the flaxseed-derived BF. The parameters investigated included solid-to-liquid ratio, extraction temperature, agitation speed, residence time, NaCl concentration, and dilution injection mode. The addition of NaCl was specifically examined for its potential to augment polysaccharide extraction by promoting solubilization and mass transfer while limiting the formation of a viscous gel layer that could hinder diffusion.

The experimental design and statistical analysis were performed using NEMRODW software. A screening design was adopted to identify the most important factors while minimizing the number of experimental runs. The studied variables and their corresponding levels are summarized in **Table 2**.

Each extract was subsequently evaluated on both phosphate PC and PS under identical conditions, using a fixed specific consumption of 200 g/t and an injection concentration of 1 g/L. Flocculation performance was assessed based on sedimentation velocity measurements.

Table 2. Investigated operating variables and experimental levels

| Variable | Code | Unit | Levels | |
|---|---|---|---|---|
| | | | -1 | 1 |
| Seed input quantity | X1 | g/l | 30 | 70 |
| Temperature | X2 | °C | 60 | 95 |
| Agitation speed | X3 | rpm | 100 | 350 |
| Residence time | X4 | min | 20 | 60 |
| NaCl quantity | X5 | g | 0 | 1 |
| Dilution injection point | X6 | - | onto residue | Into filtrate |

#### 2.6.3. Model validation procedure

Model validation was performed through three independent extraction tests conducted under the optimised unified conditions for PC and PS. For each test. The sedimentation velocity obtained value was determined at a fixed dosage of 200 g/t and an injection concentration of 1 g/L. The experimentally obtained values were subsequently compared with those predicted by the corresponding regression models.

The predictive accuracy of the models was assessed using the relative error, calculated according to **Błąd! Nie można odnaleźć źródła odwołania.**:

$$\text{Relative Error (\%)} = \frac{|V_{exp} - V_{pred}|}{V_{pred}} \times 100 \quad (6)$$

where $V_{exp}$ represents the experimental sedimentation velocity (cm/min) and, $V_{pred}$ denotes the predicted sedimentation velocity.

#### 2.6.4. Optimization of flocculant injection concentration

The injection concentration of the flocculent is a critical parameter governing flocculation efficiency, as it directly affects polymer dispersion, particle-polymer interactions, and subsequent floc formation (Bolto &

Gregory, 2007). To investigate this effect, sedimentation tests were therefore conducted on both PC and PS matrices at a fixed specific consumption of 200 g/t, while systematically varying the injection concentration.

For each experimental condition, the settling rate was measured and analyzed. The objective of this study is to identify optimal injection concentration by jointly considering performance and practical industrial constraints, particularly those associated with water availability.

#### 2.6.5. Determination of optimal BF dosage

Following the section of the most effective extract and the optimization of the injection concentration, the optimal specific consumption of the BF was determined. Initially, sedimentation tests were conducted using industrial synthetic flocculants under reference conditions (Table 1), and the corresponding settling rates were used as benchmark values.

Subsequently, the selected BF was evaluated over a range of dosages while maintaining the injection concentration at its previously optimized level. For each dosage, the settling rate was measured and systematically compared with that of the reference synthetic flocculant.

The optimal dosage was defined as the minimum amount required to achieve a sedimentation rate equal to or greater than the benchmark value, thereby ensuring comparable or improved performance.

### 2.7. Flocculant–particle interaction and floc characterization

#### 2.7.2. Structural characterization of flocculants

The functional groups present in the raw materials and prepared mortars were determined by Fourier Transform Infrared (FTIR) spectroscopy using an FTIR-4600 spectrometer (JASCO Corporation, Japan). Spectra were recorded over the wavenumber range of 4000 - 400 $cm^{-1}$.

#### 2.7.3. Phytochemical profiling of the BF

The phytochemical composition of the BF extract was characterized using high-performance liquid chromatography coupled with photodiode array detection and tandem mass spectrometry (HPLC-PDA-MS/MS). Analyses were performed on a SHIMADZU LC-MS 8050 system with an electrospray ionization (ESI) source operating in negative ion mode.

Chromatographic separation was achieved on a C18 column (Zorbax Eclipse XDB-C18, 4.6 × 150 mm, 3.5 μm). The mobile phase consisted of water and acetonitrile, both acidified with 0.1% formic acid. Two gradient elution programs were employed:

- a full-scan method ranging from 5 to 90% acetonitrile over 60 min) and
- an optimized method ranging from 15 to 90% acetonitrile over 30 min, followed by a 10 min hold at 90%.

In both cases, the flow rate was maintained at 1 mL/min.

Samples were introduced using an autosampler, and data acquisition and processing were performed using LC Solution.

#### 2.7.4. Zeta potential measurements

Zeta potential measurements were performed to evaluate the surface charge properties of PC and PS, as well as their interaction with BF. The zeta potential was initially determined at pH 3, 7, and 11, with pH adjustments performed using dilute HCl (1%) and NaOH (1%) in order to characterize surface charge behavior and potential electrostatic interactions.

Subsequently, the effect of BF dosage was investigated at neutral pH (pH 7), representative of typical industrial conditions. All measurements were carried out using a Zetasizer Nano ZS (Malvern Panalytical, UK), based on electrophoretic light scattering, following prior homogenization of the suspensions.

## 3. Results and discussion

### 3.1. Characterization of raw materials

#### 3.1.2. Chemical composition analysis

The chemical composition of the PC and PS samples, as determined by X-ray fluorescence (XRF) analysis, is summarized in Table 3.

Table 3. Chemical composition of PC and PS determined by XRF analysis

| | P2O5 | CaO | Al2O3 | Fe2O3 | K2O | MgO | $SiO_2$ |
|---|---|---|---|---|---|---|---|
| PC | 23 % | 44,2 % | 1,89 % | 0,735 % | 0,214 % | 2 ,703 % | 8,31 % |
| PS | 17,5% | 36,3% | 3,26 % | 1,19 % | 0,29 % | 2,75 % | 15,77 % |

In Moroccan sedimentary phosphate ores, the principal valuable mineral phase is fluorapatite, which occurs in association with gangue minerals such as calcite and dolomite, as well as silicates and clay minerals. These constituents collectively define the mineralogical framework of the Moroccan phosphate matrix (Derhy et al., 2024). Based on the quantification of major oxides, particularly $P_2O_5$, MgO, and CaO, a mineralogical estimation was performed, revealing a marked difference in phase distribution between PC and PS.

The PC sample is characterized by a high apatite content (approximately 54%), accompanied by a moderate carbonate level, with calcite and dolomite contents of about 18% and 12%, respectively. The remaining fraction is primarily composed of siliceous and alumino-ferric phases, including 8.31% $SiO_2$ along with minor amounts of $Al_2O_3$ and $Fe_2O_3$.

In contrast, the PS sample exhibits a lower apatite content (approximately 41%) and a higher proportion of carbonate phases, with calcite ranging from 16 to 17% and dolomite around 13%. Additionally, the PS contains a significantly higher silicate (15.77% $SiO_2$), indicative of an enrichment in fine clayey and silicate particles.

### 3.1.3. Particle size distribution by laser diffraction

Particle size distribution analysis performed by laser diffraction revealed marked differences between the two phosphate matrices, as illustrated in **Błąd! Nie można odnaleźć źródła odwołania.** and **Błąd! Nie można odnaleźć źródła odwołania.**. The PS sample was characterized by a fine particle population, with a $D_{80}$ below 40 µm. In contrast, PC exhibited a significantly coarser distribution, with a $D_{80}$ of approximately 140 µm and a $D_{90}$ close to 165 µm (The slight depletion of the coarse fraction in the concentrate may be attributed to hydrodynamic effects occurring during industrial sampling. In slurry pipeline transport systems, particle size distribution is strongly influenced by flow conditions, as well as particle size and density. These factors promote size-dependent segregation phenomena, whereby finer particles remain preferentially suspended, while coarser particles tend to settle or migrate toward low-velocity zones (Kaushal & Tomita, 2002; Laín & Sommerfeld, 2012).

Nevertheless, the observed particle size distributions remain within the typical ranges reported for slurry transport systems.
*Table* 4).

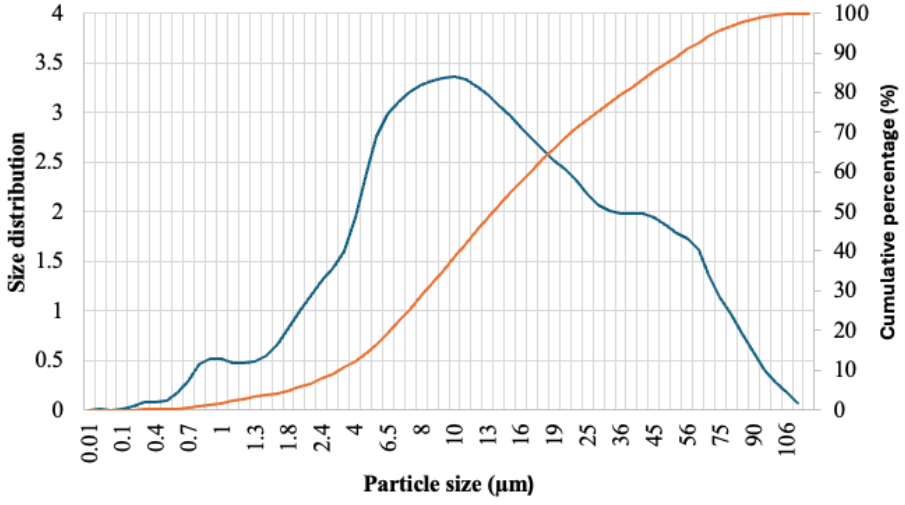


Fig. 3. Particle size distribution of PS

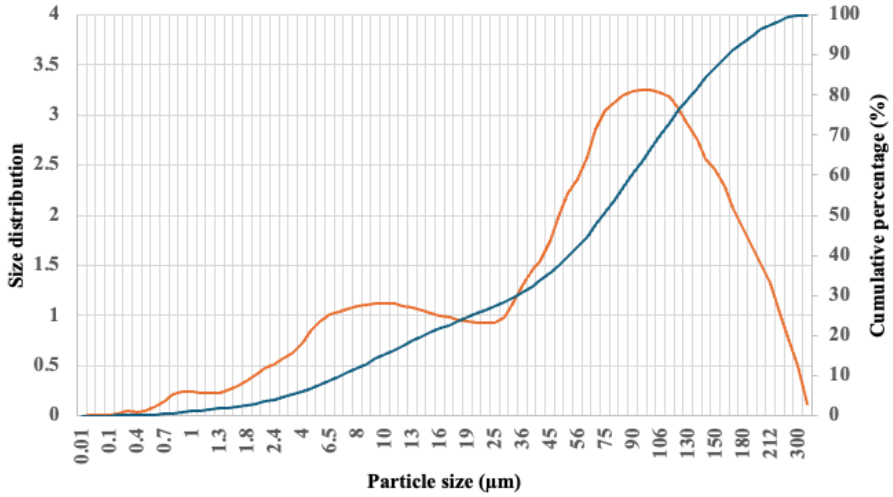


Fig. 4. Particle size distribution of PC

The slight depletion of the coarse fraction in the concentrate may be attributed to hydrodynamic effects occurring during industrial sampling. In slurry pipeline transport systems, particle size distribution is strongly influenced by flow conditions, as well as particle size and density. These factors promote size-dependent segregation phenomena, whereby finer particles remain preferentially suspended, while coarser particles tend to settle or migrate toward low-velocity zones (Kaushal & Tomita, 2002; Laín & Sommerfeld, 2012).

Nevertheless, the observed particle size distributions remain within the typical ranges reported for slurry transport systems.

Table 4. Characteristic particle diameters (D10, D50, D80, D90) of the samples studied

| | D10 | D50 | D80 | D90 |
|---|---|---|---|---|
| **PC** | 7 µm | 75 µm | 140 µm | 165 µm |
| **PS** | 2,4 µm | 12 µm | 33 µm | 53 µm |

### 3.2. Bioflocculant extraction and validation

#### 3.2.2. Screening design results

The experimental design matrix and corresponding responses for both PC and PS matrices are presented in Table 5. The effects of the investigated factors were analyzed using NEMRODW software, with the results illustrated in **Błąd! Nie można odnaleźć źródła odwołania.** and further interpreted through Pareto diagrams shown in **Błąd! Nie można odnaleźć źródła odwołania.** and **Błąd! Nie można odnaleźć źródła odwołania.**. A summary of the statistical parameters is provided in Table 6. Overall, the results indicate that the influence of the studied factors varies significantly depending on the nature of the material. For the PC, seed dosage, extraction temperature, agitation speed, and residence time exhibited positive effects on sedimentation velocity. On the other hand, the NaCl concentration and the dilution/injection mode showed negative contributions. For the PS, seed dosage, extraction temperature, agitation speed, and NaCl concentration had positive effects, whereas residence time and dilution/injection mode negatively impacted the response.

Pareto analysis **Błąd! Nie można odnaleźć źródła odwołania.** identified extraction temperature as the most influential factor for both matrices. In the case of PC, the subsequent factors in order of decreasing importance were seed dosage, dilution/injection mode, agitation speed, NaCl concentration, and residence time. For PS, temperature remained dominant, followed by agitation speed, residence time, seed dosage, and NaCl concentration, while the dilution/injection mode had negligible effect.

The cumulative effects (**Błąd! Nie można odnaleźć źródła odwołania.**) further confirmed that extraction temperature and seed dosage are the predominant factors governing the response in both

matrices. Additionally, the dilution injection mode contributed significantly to the PC, whereas agitation speed and residence time played a more prominent role for the PS.

Model statistics (Table 6) demonstrated excellent fitting performance, with coefficients of determination $R^2$ values exceeding 99% for both matrices and high reproducibility levels (above 99% for PC and above 93% for PS), thereby confirming the robustness and reliability of the experimental design. These results provide a solid basis for mechanistic interpretation, linking operating conditions to the extraction efficiency of active macromolecular species and their subsequent impact on flocculation performance.

The extraction temperature significantly enhanced the flocculation efficacy of both matrices. **Błąd! Nie można odnaleźć źródła odwołania.** illustrates that elevating the extraction temperature from 60 to 95 °C markedly improved flocculation efficiency, suggesting that extracts procured at the higher temperature demonstrated enhanced performance. This enhancement is due to improved mucilage solubilization and more effective mass transfer between the solid matrix (the seeds) and the aqueous phase, with water serving as the extraction solvent, thus facilitating the release of bioactive compounds responsible for flocculation. While increased temperatures can cause structural alterations or partial degradation of polysaccharides, as reported in the literature (Shen et al., 2010), the current findings suggest that, under the examined experimental conditions, the enhancement in extraction efficiency surpasses the possible impacts of thermal degradation. The Pareto analysis (**Błąd! Nie można odnaleźć źródła odwołania.**) further substantiates this interpretation by distinctly identifying extraction temperature as the predominant factor influencing the flocculation response in both matrices.

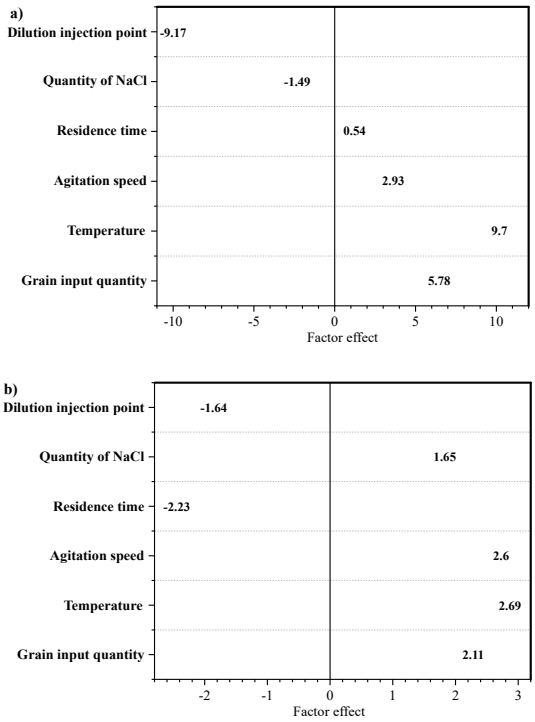


Fig. 5. Graphical analysis of factor effects for (a) PC and (b) PS

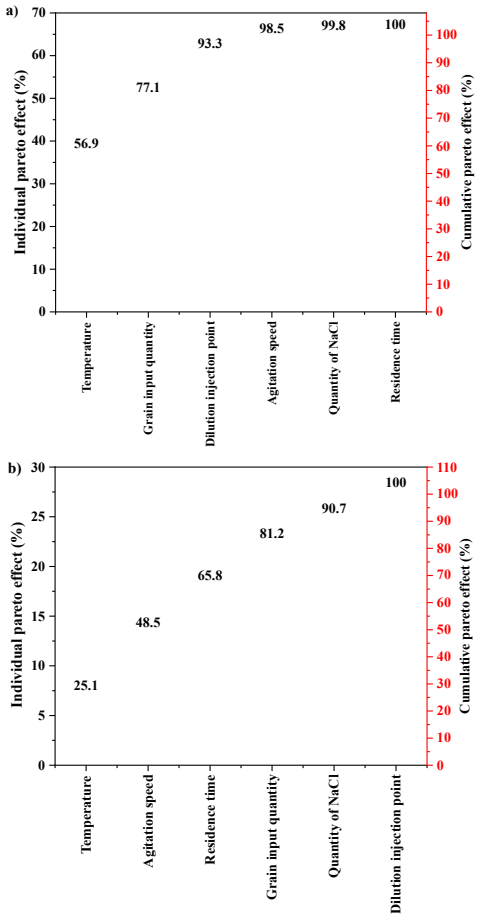


Fig. 6. Individual and cumulative Pareto effects for (a) PC and (b) PS

Table 5. Experimental design and measured responses for PC and PS

| N°Exp | Grain imput quantity | Temperature | Agitation speed | Residence time | Quantity of NaCl | Dilution injection point | Sedimentation velocity for PC | Sedimentation velocity for PS |
|---|---|---|---|---|---|---|---|---|
| | g/l | °C | RPM | min | g/l | | cm/min | cm/min |
| 1 | 70 | 95 | 350 | 20 | 1 | onto residue | 150.00 | 10.00 |
| 2 | 30 | 95 | 350 | 60 | 0 | into filtrate | 59.86 | 8.75 |
| 3 | 30 | 60 | 350 | 60 | 1 | onto residue | 46.59 | 7.78 |
| 4 | 70 | 60 | 100 | 60 | 1 | into filtrate | 43.18 | 5.00 |
| 5 | 30 | 95 | 100 | 20 | 1 | into filtrate | 48.70 | 9.13 |
| 6 | 70 | 60 | 350 | 20 | 0 | into filtrate | 49.69 | 9.57 |
| 7 | 70 | 95 | 100 | 60 | 0 | onto residue | 74.65 | 8.65 |
| 8 | 30 | 60 | 100 | 20 | 0 | onto residue | 43.86 | 5.10 |

Table 6. Statistical parameters

| | **PC** | **PS** |
|---|---|---|
| **Standard deviation of the response** | 1.7571604 | 1.4813887 |
| **$R^2$** | 99.8 % | 99.1 % |
| **Adjusted $R^2$** | 98.4 % | 93.4 % |

Seed dosage also showed a pronounced positive effect. Lower doses resulted in reduced flocculation efficiency, while higher dosages significantly enhanced sedimentation performance. This confirms that the amount of active polysaccharidic macromolecules controls BF efficiency. An increased polymer concentration promotes stronger polymer-particle interactions, leading to the formation of larger and denser flocs. This behavior is consistent with the bridging mechanism commonly described for polymeric flocculants (Bolto & Gregory, 2007; Salehizadeh & Shojaosadati, s. d.).

The dilution mode exhibited a consistent effect across both matrices. The addition of dilution water directly to the extraction residue proved more effective than dilution of the filtrate. This finding suggests that a fraction of the active macromolecules remain associated with the solid matrix after the initial extraction step. The additional dilution step facilitates desorption and recovery of these compounds, thereby enhancing the quality of the final extract. This behavior can be explained by solid–liquid equilibrium and mass transfer mechanisms commonly encountered in natural product extraction processes (Chemat et al., 2012).

The impact of agitation was determined to be contingent upon the matrix. In the PC matrix, agitation exerted a relatively constrained impact, primarily enhancing the dispersion of the extracted polymer in the solution, with only a negligible effect on flocculation efficacy. Conversely, in the PS matrix, agitation augmented mass transfer during the extraction process, leading to a more efficient release of mucilage and a more significant enhancement in flocculation performance. This disparity may be ascribed to the unique mineralogical properties of the two matrices. Increasing agitation intensity specifically enhances the extraction of compounds with low flocculating activity in the PC matrix, while in the PS matrix, it promotes the release of more active compounds, elucidating the observed differences between the two matrices.

The influence of NaCl concentration differed between two systems. In the PC matrice, increasing ionic strength exerted a moderate negative effect, likely due to conformational changes in polymer chains that reduce their extension and bridging capacity in solution (Bolto & Gregory, 2007). Conversely, for PS, NaCl additionally increased sedimentation velocity by compressing the electrical double layer, thereby reducing electrostatic repulsion and promoting particle aggregation. Under these conditions, colloidal destabilization mechanisms appear to dominate over polymer conformational effects.

Residence time also exhibited matrix-dependent behavior. In the PC system, its impact was limited, signifying the swift achievement of extraction equilibrium. In contrast, in the PS system, prolonged residence time significantly reduced sedimentation performance, suggesting that extended extraction does not improve the recovery of active compounds and may even impair flocculation efficiency. This behavior may be attributed to partial polymer degradation or conformational changes. These results indicate that moderate extraction times are sufficient to obtain an effective BF.

Overall, the impact of operating parameters differs between PC and PS due to variations in their chemical composition (Table 3). However, the convergence of the most influential factors suggests that a unified extraction process can be implemented on an industrial scale. The results of the comparative analysis and the selected operating conditions are summarized in Table 7, where optimal parameter levels were identified to ensure both high process performance and industrial feasibility.

Table 7. Comparative analysis of operating parameters and optimal conditions for PC and PS

| Factor | Effect Direction | | Pareto Effect | | Unified Extraction Process |
|---|---|---|---|---|---|
| | For PC | For PS | For PC | For PS | |
| Seed input quantity | Positive | Positive | 20.19 | 15.48 | 70 |
| Temperature | Positive | Positive | 56.92 | 25.1 | 95 |
| Agitation speed | No significant effect | Positive | | 23.45 | 350 |
| Residence time | No significant effect | Negative | | 17.21 | 20 |
| NaCl quantity | No significant effect | No significant effect | | | 0 |
| Dilution injection point | Negative | No significant effect | 16.18 | | Residue |
| | | | 93.29 | 81.24 | |

### 3.2.3. Model validation analysis

Mathematical models correlating the operating variables with sedimentation velocity were developed based on experimental data obtained for both matrices. The resulting models for PC and PS matrices are presented in **Błąd! Nie można odnaleźć źródła odwołania.** and **Błąd! Nie można odnaleźć źródła odwołania.**, respectively. Experimental sedimentation velocities were determined through laboratory tests and subsequently compared with the values predicted by the developed models.

$$Y = 55.529 + 5.776B1 + 9.669B2 + 2.931B3 + 0.541B4 - 1.486B5 - 5.171B6 \quad (7)$$

$$Y = 9.764 + 2.111B1 + 2.689B2 + 2.599B3 - 2.226B4 + 1.651B5 - 1.636B6 \quad (8)$$

The results of the unified extraction process are summarised in Table 8. A close agreement was observed between experimental and predicted values for both PC and PS matrices. The calculated relative errors stay within acceptable limits, thereby confirming the accuracy and reliability of the proposed models.

Table 8. Comparison of experimental and predicted sedimentation velocities under the unified extraction process

| | Test | Experimental Velocity (cm/min) | Average sedimentation velocity (cm/min) | Predicted Velocity (cm/min) | Relative error (%) |
|---|---|---|---|---|---|
| PC | 1 | 80.407 | 80.113 | 80,021 | 0.11 |
| | 2 | 79.923 | | | |
| | 3 | 80.010 | | | |
| PS | 1 | 19.392 | 19.349 | 19.374 | 0.13 |
| | 2 | 19.306 | | | |
| | 3 | 19.350 | | | |

### 3.3. Effect of injection concentration on bioflocculation performance

Fig. 5 illustrates the variation in sedimentation velocity as a function of BF injection concentration for PS and PC at a fixed dosage of 200 g/t, using the unified extraction process. The results reveal two distinct regimes: a moderate increase in sedimentation velocity in the 1-2 g/L range and a more pronounced improvement within the 0.1–1 g/L interval.

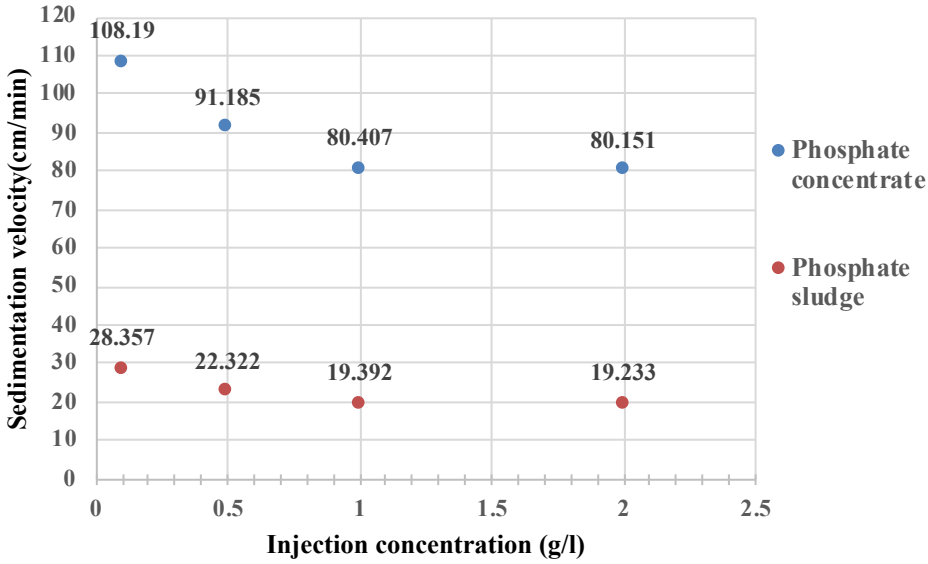


Fig. 5. Effect of injection concentration on sedimentation velocity

This behavior highlights the critical role of injection concentration in governing flocculation efficiency. The observed trends can be interpreted in terms of polymer conformation: dilution promotes

polymer chain extension and enhances interparticle bridging, whereas higher concentrations favor chain entanglement and steric hindrance, thereby reducing flocculation efficiency (Bolto & Gregory, 2007; Lee et al., 2014).

From a process engineering standpoint, although increased dilution improves settling kinetics, it significantly raises water demand. This constraint is particularly relevant in mineral processing operations, where water availability is often limited, especially in arid regions (Gunson et al., 2012; Mudd, 2008; Northey et al., 2016). Excessive dilution also leads to higher volumetric flow rates entering industrial thickeners or decanters. At very high dilution levels, the flow rate of the flocculant solution may approach that of the pulp stream, which deviates from standard operating conditions where flocculant flow rates are typically negligible compared to slurry flow rates.

Based on a trade-off between sedimentation performance, reagent consumption, hydraulic load, and water availability, an injection concentration of 0.5 g/L was identified as the optimal operating condition. This value ensures high flocculation efficiency while remaining compatible with industrial constraints.

### 3.4. Determination of bioflocculant specific consumption under optimized operating conditions

Fig. 6 and Fig. 7 present the effect of BF dosage on the sedimentation velocity of PC and PS, respectively, along with a comparison to conventional synthetic flocculants (SFC and SFS). In both matrices, sedimentation velocity increased with increasing BF dosage, indicating that higher polymer concentrations enhance particle aggregation, leading to the formation of larger and denser flocs with improved settling behavior. For the PC, a BF dosage of 400 g/t resulted in a sedimentation velocity of 130.79 cm/min, slightly exceeding the performance of SFC, which achieved 128.51 cm/min at a dosage of 16 g/t. In the PS, a BF dosage of 205 g/t yielded a sedimentation velocity of 24.10 cm/min, comparable to that of SFS (23.19 cm/min at 11 g/t).

These results are consistent with previous studies demonstrating that flaxseed-derived bioflocculants, rich in high-molecular-weight polysaccharides, promote particle aggregation primarily through adsorption and bridging mechanisms (Kučka et al., 2024; Venegas-García & Wilson, 2022). Comparable findings have been reported in phosphate tailings, where flaxseed mucilage improves water recovery and sludge densification, thereby supporting its potential as a sustainable substitute for synthetic flocculants (Ettoumi et al., 2025).

Overall, the results demonstrate that the BF exhibits flocculation performance comparable to that of industrial synthetic flocculants, highlighting its potential as an environmentally friendly solution for phosphate slurry treatment.

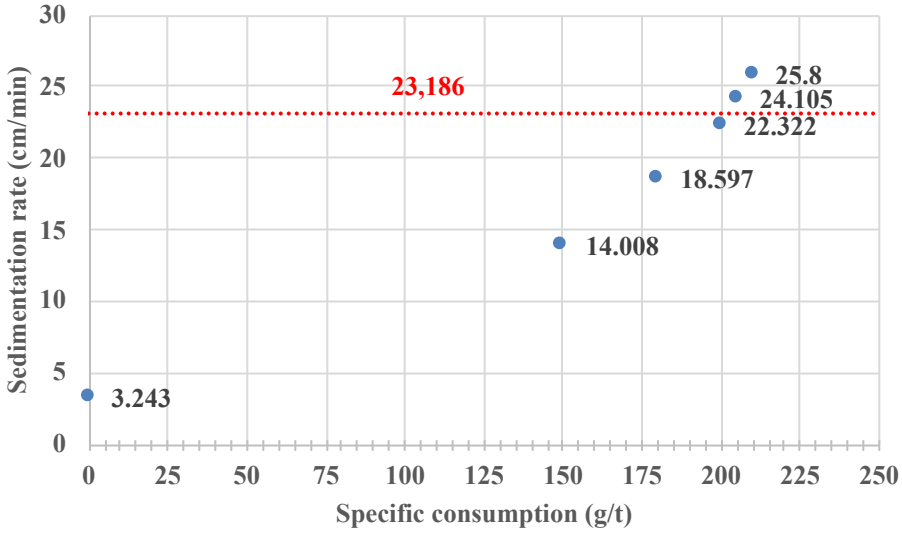


Fig. 6. Effect of BF dosage on sedimentation velocity for PS (comparison with SFS)

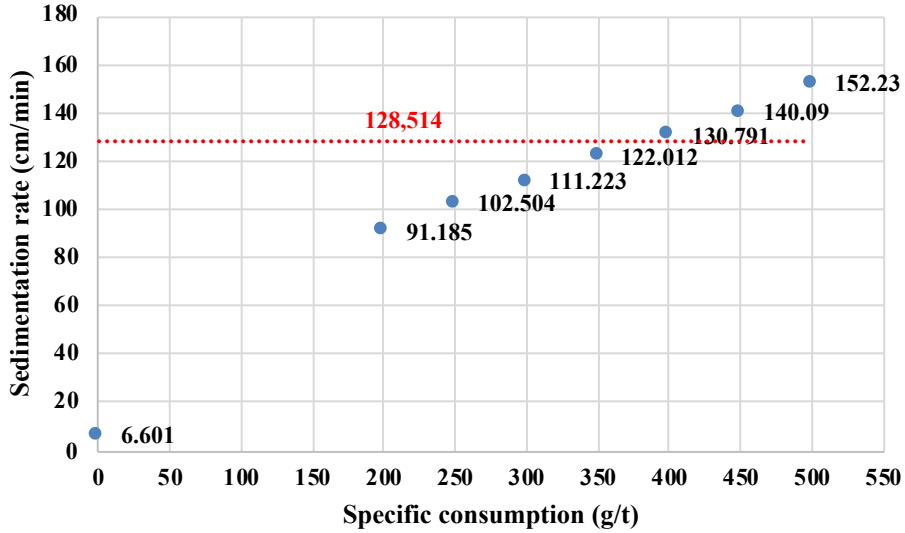


Fig. 7. Effect of BF dosage on sedimentation velocity for PC (comparison with SFC)

### 3.5. Chemical characterization of the bioflocculant

#### 3.5.2. FTIR characterization of the bioflocculant

FTIR analysis was performed on both the raw and water-corrected spectra of the BF extract (**Błąd! Nie można odnaleźć źródła odwołania.**). In aqueous systems, intense absorption bands associated with water, typically observed around 3300 and 1635 $cm^{-1}$, can dominate the spectrum and obscure weaker signals originating from bioactive compounds. In the present study, water interference significantly reduced peak visibility, therefore, a spectral correction was applied to minimize its contribution. This approach enabled the identification of low-intensity bands that were previously masked, thereby improving the interpretation of the extract composition (Skinner et al., 2012; Zhang et al., 2022).

The FTIR spectrum of the raw extract exhibited a broad band near 3300 $cm^{-1}$ and a distinct peak around 1635 $cm^{-1}$, corresponding to O–H stretching and H–O–H bending of water, respectively. These strong absorptions can mask characteristic signals from the extract constituents and may overlap with functional groups containing hydroxyl moieties, such as polyphenols, organic acids, and carbohydrates. Consequently, certain compositional features of the extract are likely concealed within these areas.

Following water subtraction, additional bands became discernible. The peaks observed at 2982 and 2900 $cm^{-1}$ were attributed to asymmetric and symmetric C–H stretching vibrations of aliphatic groups, indicating the presence of hydrocarbon chains. The band at 1404 $cm^{-1}$ was assigned to O–H bending and aromatic C=C vibrations, suggesting the presence of phenolic structures. Furthermore, the peak at 1049 $cm^{-1}$ corresponds to C–O stretching vibrations, characteristic of alcohols, esters, and glycosidic linkages.

Although the overall band intensities remain relatively low due to the dilute nature of the extract and the initial presence of water, the spectral subtraction procedure significantly enhances the detection of functional groups. This provides a more accurate and comprehensive characterization of the chemical composition of the BF extract.

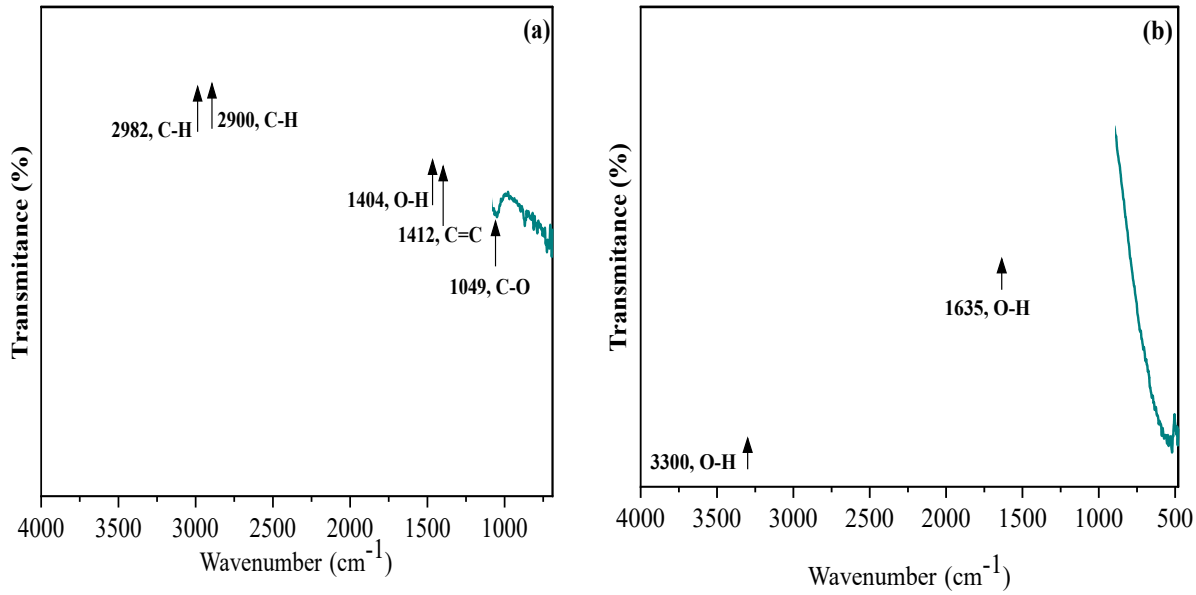


Fig. 10. FTIR spectra of the extracted BF: (a) the original spectrum and (b) the spectrum after removal of water interference

### 3.5.3. HPLC analysis of bioactive compounds in the bioflocculant

The chemical composition of the flaxseed-derived extract was investigated by HPLC-MS analysis operating in negative ionization mode. Chromatographic profiles obtained from two independent injections are presented in **Błąd! Nie można odnaleźć źródła odwołania.**, highlighting the reproducibility of the analytical method. The identified compounds are listed in

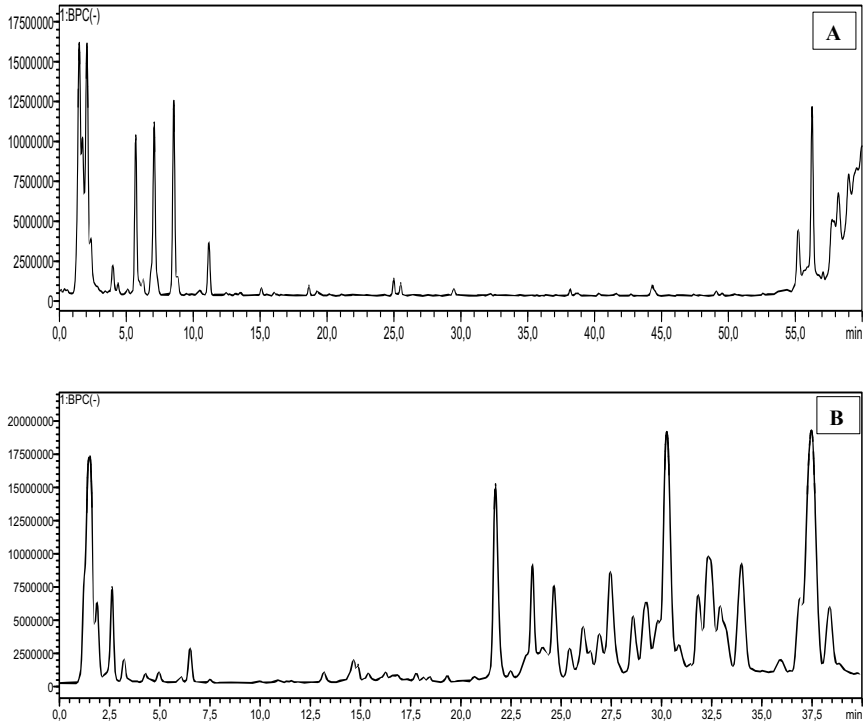


Fig. 11. HPLC/MS chromatographic profiles of the flaxseed extract showing two independent injections

*Table 9*.

The HPLC/MS results revealed a chemically diverse extract composed of organic acids, phenolic compounds, flavonoids, lignans, and lipid derived species. Early eluting compounds were predominantly low-molecular-weight organic acids, including citric, malic, tartaric, and galactaric, which may influence surface charge and intermolecular interactions. A substantial fraction of the

detected species corresponded to phenolic acids and their glycosylated derivatives, such as caffeic, gallic, ferulic, protocatechuic, and hydroxycinnamic acid derivatives.

In addition, several flavonoids were identified, including (epi)catechin, kaempferol diglucoside, isorhamnetin, and apigenin derivatives, confirming the presence of bioactive polyphenolic compounds. Lignan-type compounds, including matairesinol and pinoresinol derivatives, characteristic constituents of flaxseed, were also detected. Furthermore, the presence of fatty acids, glycerol derivatives, ceramides, and phospholipid-like compounds at higher retention times underscores the composition complexity of the extract (Herchi et al., 2014; Kajla et al., 2015; Popova et al., 2009).

These results are in line with FTIR analysis, which indicated a wide range of chemical functionalities within the extract. The identification of organic acids, phenolic compounds, and flavonoids by HPLC-MS correlates with infrared absorption bands associated with hydroxyl (–OH), carbonyl (C=O), and C–O functional groups. In particular, the broad O–H stretching band and the signals in the 1600–1000 $cm^{-1}$ region support the presence of polyphenolic structures and oxygenated functional groups. But strong water-related absorption bands around 3300 $cm^{-1}$ and 1635 $cm^{-1}$ may overlap with characteristic signals, potentially masking certain functional groups.

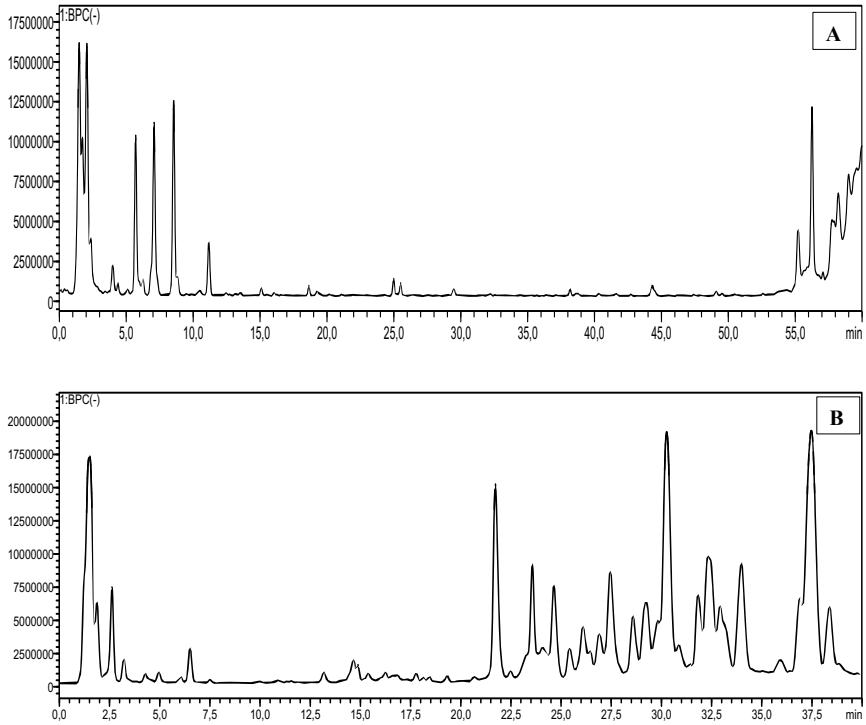


Fig. 11. HPLC/MS chromatographic profiles of the flaxseed extract showing two independent injections

Table 9. Annotated compounds from flaxseed extract using HPLC/MS

| Rt (min) | [M-H] - | MS/MS | Proposed compounds |
|---|---|---|---|
| **0.37** [a] | 208 | 128 | Pyroglutamic acid sulfate |
| **1.07** [a] | 191 | 111 | (Iso) Citric acid |
| **1.08** [a] | 133 | 133 | Malic acid |
| **1.20** [b] | 159 | 115 | Oxoadipic acid |
| **1.28** [a] | 289 | 289 | (Epi)Catechin |
| **1.57** [a] | 209 | 191 | Galactaric acid |
| **1.61** [a] | 149 | 103 | Tartaric acid |
| **1.68** [a] | 341 | 179 | Caffeic acid glucoside |
| **1.81** [a] | 503 | 179 | Caffeic acid diglucoside |
| **2.22** [a] | 191 | 111 | Citric acid |
| **2.55** [a] | 187 | 125, 169 | Gallic acid monohydrate |
| **2.87** [a] | 289 | 125 | (Epi)Catechin |

| | | | |
|---|---|---|---|
| **2.88** [a] | 173 | 129 | Shikimic acid |
| **3.37** [a] | 453 | 169 | Gallic acid derivative |
| **3.98** [a] | 331 | 125 | Galloylglucose |
| **4.65** [a] | 169 | 125 | Gallic acid |
| **4.87** [a] | 315 | 153 | Dihydroxybenzoic acid glucoside |
| **5.77** [a] | 467 | 179 | Caffeic acid rhamnosyl-glucoside |
| **6.61** [a] | 487 | 307 | Syringyl glucose derivative |
| **6.64** [a] | 153 | | Dihydroxybenzoic acid |
| **6.85** [a] | 315 | 153 | Protocatechuic acid glucoside |
| **7.94** [a] | 325 | 163 | Hydroxycinnamic glucoside |
| **9.20** [a] | 299 | 137 | Hydroxybenzoic acid glucoside |
| **10.34** [a] | 355 | 135 | Caffeoyl glucuronide |
| **10.75** [a] | 295 | 137 | Hydroxybenzoic acid derivative |
| **10.89** [a] | 295 | 119 | Hydroxycinnamic pentose |
| **11.08** [a] | 159 | 115 | Oxoadipic acid |
| **11.25** [a] | 325 | 163 | Hydroxycinnamic glucose |
| **11.45** [a] | 179 | 135,179 | Caffeic acid |
| **12.60** [b] | 329 | 193 | Ferulic acid glucoside |
| **12.80** [a] | 549 | 179 | Caffeic acid derivative |
| **14.24** [b] | 315 | 271 | Isorhamnetin |
| **14.91** [a] | 551 | 163 | Hydroxycinnamic glucoside derivative |
| **14.59** [a] | 449 | 311 | Caftaric acid derivative |
| **16.87** [b] | 357 | 221 | Matairesinol/ Pinoresinol |
| **18.75**[a] | 163 | | Coumaric acid |
| **19.97** [a] | 161 | 133 | Hydroxycummarin |
| **20.52** [b] | 339 | 293, 311 | Ethyl icosanoate |
| **21.62** [b] | 265 | | Dodecyl sulfate |
| **22.78** [a] | 609 | 285 | Kaempferol diglucoside |
| **23.32** [a] | 331 | 179 | Caffeic acid gallate |
| **24.49** [b] | 279 | | Linoleic acid |
| **24.74** [b] | 639 | 277 | Ceramides derivative |
| **27.36** [b] | 377 | 265, 293 | 2-Arachidonoyl glycerol |
| **28.03** [a] | 853 | 269 | Apigenin derivative |
| **28.26** [b] | 353 | 293 | Linoleoylglycerol |
| **30.02** [b] | 451 | 339, 405 | decyl icosanoate |
| **30.15** [b] | 645 | 339 | Ceramides derivative |
| **30.27** [b] | 621 | | Ceramides derivative |
| **30.31** [b] | 743 | 279, 317, 607 | Glycerophospholipids derivative |
| **31.26** [a] | 429 | 163 | Hydroxycinnamic derivative |
| **33.02** [b] | 983 | 279 | Linoleic acid derivative |
| **36.75** [b] | 655 | 255, 279, 636 | Ceramides derivative |
| **36.88** [b] | 353 | | Linoleoylglycerol |
| **37.16** [b] | 819 | 277 | Glycerophospholipids derivative |
| **37.57** [b] | 311 | 265 | Icosanoic acid |
| **37.41** [b] | 325 | 183, 197 | Methyl icosanoate |
| **38.19** [b] | 307 | | Dihomolinoleic acid |
| **39.38** [b] | 339 | 293, 311 | Ethyl icosanoate |
| **58.02** [a] | 563 | 253, 281 | Ceramides derivative |

[a]: Rt (min) in method a, [b]: Rt (min) in method b

### 3.6. Zeta potential analysis

Fig. 8 shows the variation of zeta potential as a function of pH for the BF, as well as for the two solid matrices, PS and PC. The findings indicate that all materials exhibit negative surface charges over the examined pH range, including acidic (pH = 3), neutral (pH = 7), and alkaline (pH = 11) conditions.

For the BF, the zeta potential shows a slight decrease between pH 3 and pH 7, followed by a more pronounced decrease under alkaline pH conditions. In contrast, both phosphate samples display a continuous decrease in zeta potential with increasing pH, reflecting a progressive increase in surface negativity. At acidic pH (pH = 3), PS and PC exhibit comparable zeta potential values, suggesting limited differentiation in surface charge under these conditions. However, as the pH increases, a clear divergence emerges, with PS exhibiting significantly more negative zeta potential values than PC, especially at neutral and alkaline pH.

This behavior can be attributed to differences in the mineralogical composition (Table 3). At low pH, surface functional groups are protonated, minimizing charge disparities between the two materials. With increasing pH, deprotonation leads to the generation of negatively charged surface sites, especially in PS, which is enriched in siliceous and clay minerals. Conversely, in the apatite-rich PC, the presence of calcium ions contributes to partial charge compensation, resulting in a comparatively less negative surface.

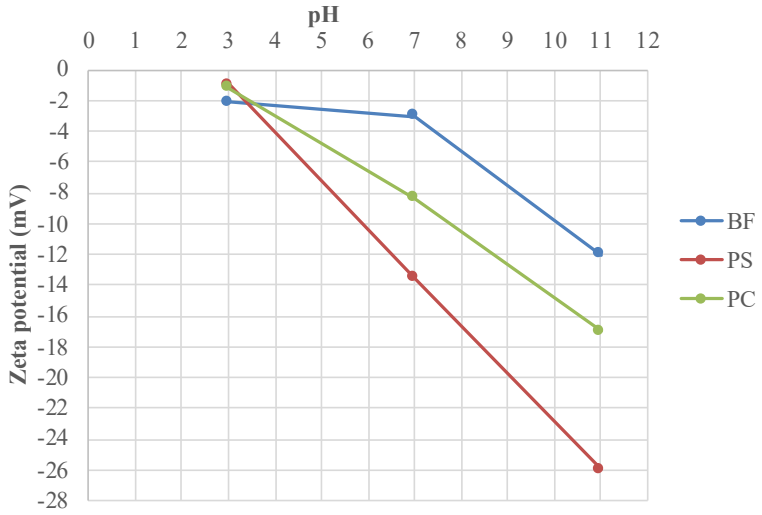


Fig. 8. Surface charge behavior of BF and phosphate solids as a function of pH

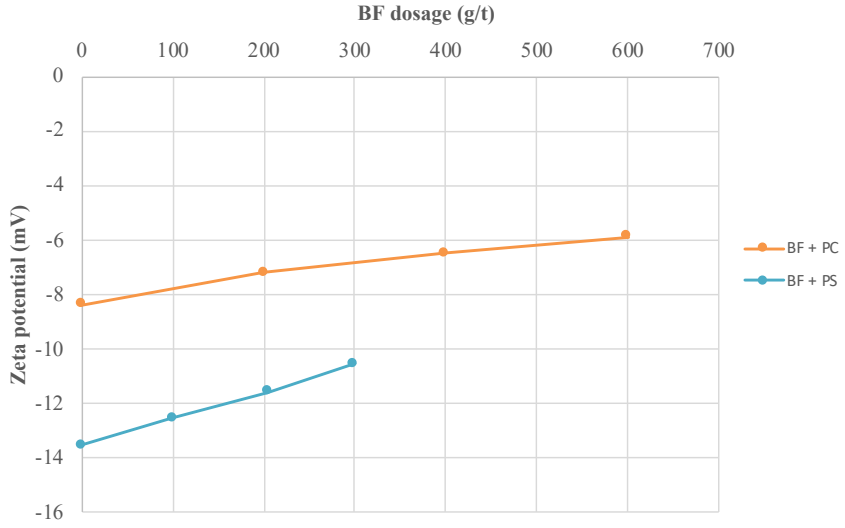


Fig. 9. Influence of BF dosage on surface charge of phosphate suspensions

Fig. 9 shows how the effect of BF dosage on zeta potential at a neutral pH (pH = 7) is considered for three dosage levels: suboptimal, optimal, and excessive. The findings indicate that increasing BF dosage

leads to a progressive elevation of zeta potential values for both matrices. However, the zeta potential remains negative and significantly distant from zero across all tested conditions. Moreover, PS exhibits lower (more negative) zeta potential values than PC. Even at the optimal dosages (205 g $t^{-1}$ for PS and 400 g $t^{-1}$ for PC), the zeta potential values remain negative.

### 3.7. Flocculant contribution analysis

Table 10 presents the calculated sedimentation velocities achieved with and without flocculant, at a dosage of 200 g/t and an injection concentration of 1 g/L, utilizing a unified extraction process. The associated flocculant contribution is also documented. The diminished contribution noted for the PS can be ascribed to its mineral composition and enhanced colloidal stability.

As indicated in Table 3, the enrichment of PS in silicate phases and metal oxides results in more negatively charged surfaces, which enhances electrostatic repulsion and reduces flocculation efficiency (Bolto & Gregory, 2007). This interpretation is supported by zeta potential measurements (Fig. 9), which show that PS has a more negative surface charge than PC. Furthermore, the addition of NaCl consistently improves flocculation performance by increasing ionic strength and compressing the electrical double layer, thereby reducing electrostatic repulsion (Bolto & Gregory, 2007).

Despite its finer particle size (D80 = 33 μm), the PS exhibits a lower flocculant contribution compared to the concentrate. This observation shows that surface area alone does not govern flocculation charges through polymer adsorption and bridging mechanisms. The elevated negative surface charge of PS likely restricts polymer adsorption and diminishes polymer chain extension, consequently reducing the efficacy of interparticle bridging (Gregory & Barany, 2011). The PC characterised by coarser particles (D80 = 140 μm) and lower surface charge promotes more effective polymer-particle interactions, resulting in enhanced flocculation performance (Gregory & Barany, 2011).

Table 10. Flocculant contribution to sedimentation performance

| | Sedimentation Velocity (Flocculant) (cm/min) | | |
|---|---|---|---|
| | Without | With | Flocculant Contribution (%) |
| PC | 6.60 | 80.40 | 91,8 |
| PS | 3.24 | 19.39 | 83,3 |

### 3.8. Flocculation mechanism

The flocculation mechanism can be inferred from the combined analysis of process performance, physicochemical characterization, and surface charge measurements. The effect of NaCl, together with the higher colloidal stability of PS associated with its silicate-rich composition, underscores the critical role of electrostatic interactions in controlling particle dispersion. Zeta potential measurements indicate that PS, PC, and the BF exhibit negative surface charges at neutral pH and that the overall system remains negatively charged following BF addition. This observation rules out charge neutralization as the dominant flocculation mechanism.

The chemical composition of the BF extract, as supported by FTIR analysis, indicates the presence of multifunctional organic molecules bearing active functional groups capable of interacting with mineral surfaces. The observed improvement in sedimentation performance, despite persistent electrostatic repulsion, indicates that flocculation is primarily governed by a polymer bridging mechanism. This process is facilitated by physicochemical interactions, such as hydrogen bonding between functional groups of the polymer and mineral surfaces.

This interpretation is consistent with previous studies on flaxseed-derived and plant-based bioflocculants (Ettoumi et al., 2025), which report that flocculation is predominantly governed by polymer bridging rather than charge neutralization. Notably, effective aggregation has been observed even in negatively charged systems, confirming the predominance of this mechanism.

In addition, studies on natural bioflocculants have shown that macromolecular compounds can adsorb onto multiple particle surfaces, forming interparticle bridges that promote floc formation

(Salehizadeh & Shojaosadati, s. d.). These interactions are further reinforced by secondary mechanisms such as hydrogen bonding, complexation, and ion-mediated effects (Bolto & Gregory, 2007), which are particularly relevant in mineral systems where electrostatic repulsion remains significant.

## 4. Conclusions

This study demonstrates that a flaxseed-derived BF can be efficiently produced through a simple and scalable aqueous extraction process and successfully applied to solid–liquid separation in mineral processing. The implementation of a design of experiments approach enabled the identification of the key parameters governing both extraction and flocculation performance, leading to the establishment of a unified set of operating conditions applicable to both PC and PS matrices.

The findings demonstrate that, despite variations in mineralogical composition and particle size distribution, a singular optimized extraction protocol can produce a BF that provides superior sedimentation performance in both matrices. The parameters examined revealed that seed dosage, extraction temperature, agitation speed, and residence time are the most significant factors affecting process efficiency.

From an application standpoint, the BF achieved sedimentation performances comparable to those obtained with conventional synthetic flocculants, thereby confirming its potential as a viable alternative for industrial use. In addition, the proposed approach relies on a straightforward extraction process that does not require complex purification or solvent-based steps, which enhances its scalability and operational feasibility.

Overall, this study provides a robust and practical framework for the development and implementation of plant-based bioflocculants in mineral processing. The combination of process simplicity, high performance, and environmental compatibility positions this approach a promising solution for sustainable water management and tailings treatment in the mining industry.

## References

ARENAS-COLLAO, K., VALDÉS-GONZÁLEZ, H., REYES-BOZO, L., SALAZAR, J. L. 2024. *The Water Management Impacts of Large-Scale Mining Operations: A Social and Environmental Perspective*. Water, 16(12), 1745.

BERGANI, A., AIT-KHOUIA, Y., EL-BAHI, A., HAKKOU, R., BENZAAZOUA, M., TAHA, Y. 2025. *Advancing sustainable dewatering of fine phosphate tailings: Evaluating xanthan gum, sodium alginate, and carboxymethyl cellulose as flocculating agents*. Water Research, 280, 123526.

BERGANI, A., TAHA, Y., AIT-KHOUIA, Y., HAKKOU, R., BENZAAZOUA, M. 2025. *Enhancing flocculation and dewatering performance of fine phosphate tailings: A sustainable approach for water resources management*. Separation and Purification Technology, 359, 130377.

BOLTO, B., GREGORY, J. 2007. *Organic polyelectrolytes in water treatment*. Water Research, 41(11), 2301–2324.

CHEMAT, F., VIAN, M. A., CRAVOTTO, G. 2012. *Green Extraction of Natural Products: Concept and Principles*. International Journal of Molecular Sciences, 13(7), 8615–8627.

CONCHA A., F. 2014. *Kynch Theory of Sedimentation*. In: *Solid-Liquid Separation in the Mining Industry*. Vol. 105. Springer International Publishing, 97–118.

DE LIMA, J. P. M., AMARAL, M. C. S., DE LIMA, S. C. R. B. 2025. *Sustainable water management in the mining industry: Paving the way for the future*. Journal of Water Process Engineering, 71, 107239.

DERHY, M., TAHA, Y., EL-BAHI, A., AIT-KHOUIA, Y., BENZAAZOUA, M., HAKKOU, R. 2024. *Selective flotation of calcite and dolomite from apatite using bio-based alternatives to conventional collectors: Castor and mustard oils*. Minerals Engineering, 208, 108597.

ELRASOUL, E. A., YONG, E. L. 2025. *A Systematic Review on the Application of Bacteria-Based Bioflocculants in Wastewater Treatment: Trends and Future Advances*. Water, Air, & Soil Pollution, 236(5), 276.

ETTOUMI, M., JOUINI, M., EL-BAHI, A., BERGANI, A., TAHA, Y., KHALIL, A., BENZAAZOUA, M. 2025. *Extraction and application of flaxseed-derived bioflocculants for phosphate tailings densification*. Journal of Water Process Engineering, 75, 108001.

GREGORY, J., BARANY, S. 2011. *Adsorption and flocculation by polymers and polymer mixtures*. Advances in Colloid and Interface Science, 169(1), 1–12.

GUNSON, A. J., KLEIN, B., VEIGA, M., DUNBAR, S. 2012. *Reducing mine water requirements*. Journal of Cleaner Production, 21(1), 71–82.

HERCHI, W., ARRÁEZ-ROMÁN, D., TRABELSI, H., BOUALI, I., BOUKHCHINA, S., KALLEL, H., SEGURA-CARRETERO, A., FERNÁNDEZ-GUTIÉRREZ, A. 2014. *Phenolic Compounds in Flaxseed: A Review of Their Properties and Analytical Methods. An Overview of the Last Decade*. Journal of Oleo Science, 63(1), 7–14.

JARVIS, P., JEFFERSON, B., GREGORY, J., PARSONS, S. A. 2005. *A review of floc strength and breakage*. Water Research, 39(14), 3121–3137.

KAJLA, P., SHARMA, A., SOOD, D. R. 2015. *Flaxseed – A potential functional food source*. Journal of Food Science and Technology, 52(4), 1857–1871.

KAUSHAL, D. R., TOMITA, Y. 2002. *Solids concentration profiles and pressure drop in pipeline flow of multisized particulate slurries*. International Journal of Multiphase Flow, 28(10), 1697–1717.

KUČKA, M., HARENČÁR, Ľ., RAŽNÁ, K., NÔŽKOVÁ, J., KOWALCZEWSKI, P. Ł., DEYHOLOS, M., DZIEDZIC, K., RYBICKA, I., ZEMBRZUSKA, J., KAČÁNIOVÁ, M., IVANIŠOVÁ, E., GAŽO, J., ČERTEKOVÁ, S., TOMKA, M. 2024. *Great potential of flaxseed mucilage*. European Food Research and Technology, 250(3), 877–893.

LAÍN, S., SOMMERFELD, M. 2012. *Numerical calculation of pneumatic conveying in horizontal channels and pipes: Detailed analysis of conveying behaviour*. International Journal of Multiphase Flow, 39, 105–120.

LEE, C. S., ROBINSON, J., CHONG, M. F. 2014. *A review on application of flocculants in wastewater treatment*. Process Safety and Environmental Protection, 92(6), 489–508.

MUDD, G. M. 2008. *Sustainability Reporting and Water Resources: A Preliminary Assessment of Embodied Water and Sustainable Mining*. Mine Water and the Environment, 27(3), 136–144.

NORTHEY, S. A., MUDD, G. M., SAARIVUORI, E., WESSMAN-JÄÄSKELÄINEN, H., HAQUE, N. 2016. *Water footprinting and mining: Where are the limitations and opportunities?* Journal of Cleaner Production, 135, 1098–1116.

ORCHARD, M. J., YANG, G., WEBBER, G. B., FRANKS, G. V., ZHAO, C.-X. 2024. *Development of bioflocculants for mineral processing*. Materials Today Sustainability, 28, 100965.

POPOVA, I. E., HALL, C., KUBÁTOVÁ, A. 2009. *Determination of lignans in flaxseed using liquid chromatography with time-of-flight mass spectrometry*. Journal of Chromatography A, 1216(2), 217–229.

SALEHIZADEH, H., SHOJAOSADATI, S. A. *Extracellular biopolymeric flocculants: Recent trends and biotechnological importance*. Biotechnology Advances, 19(5), 371-385.

SHEN, D. K., GU, S., BRIDGWATER, A. V. 2010. *The thermal performance of the polysaccharides extracted from hardwood: Cellulose and hemicellulose*. Carbohydrate Polymers, 82(1), 39–45.

SKINNER, J. L., PIENIAZEK, P. A., GRUENBAUM, S. M. 2012. *Vibrational Spectroscopy of Water at Interfaces*. Accounts of Chemical Research, 45(1), 93–100.

VENEGAS-GARCÍA, D. J., WILSON, L. D. 2022. *Utilization of Bioflocculants from Flaxseed Gum and Fenugreek Gum for the Removal of Arsenicals from Water*. Materials, 15(23), 8691.

ZHANG, X., HE, A., GUO, R., ZHAO, Y., YANG, L., MORITA, S., XU, Y., NODA, I., OZAKI, Y. 2022. *A new approach to removing interference of moisture from FTIR spectrum*. Spectrochimica Acta Part A: Molecular and Biomolecular Spectroscopy, 265, 120373.